



HAL
open science

Quantifying the Contribution of the Dispersion Interaction and Hydrogen Bonding to the Anisotropic Elastic Properties of Chitin and Chitosan

Pan Chen, Changjun Zhao, Huanyu Wang, Yiwei Li, Guoqiang Tan, Ziqiang Shao, Yoshiharu Nishiyama, Tao Hu, Jakob Wohlert

► **To cite this version:**

Pan Chen, Changjun Zhao, Huanyu Wang, Yiwei Li, Guoqiang Tan, et al.. Quantifying the Contribution of the Dispersion Interaction and Hydrogen Bonding to the Anisotropic Elastic Properties of Chitin and Chitosan. *Biomacromolecules*, 2022, 23 (4), pp.1633-1642. 10.1021/acs.biomac.1c01488 . hal-03746710

HAL Id: hal-03746710

<https://hal.science/hal-03746710>

Submitted on 5 Aug 2022

HAL is a multi-disciplinary open access archive for the deposit and dissemination of scientific research documents, whether they are published or not. The documents may come from teaching and research institutions in France or abroad, or from public or private research centers.

L'archive ouverte pluridisciplinaire **HAL**, est destinée au dépôt et à la diffusion de documents scientifiques de niveau recherche, publiés ou non, émanant des établissements d'enseignement et de recherche français ou étrangers, des laboratoires publics ou privés.

Quantifying the Contribution of Dispersion Interaction and Hydrogen Bonding to the Anisotropic Elastic Properties of Chitin and Chitosan

Pan Chen,^{*,†,||} Changjun Zhao,^{†,||} Huanyu Wang,[†] Yiwei Li,[†] Guoqiang Tan,[†] Ziqiang Shao,[†] Yoshiharu Nishiyama,^{*,‡} Tao Hu,[¶] and Jakob Wohler^{*,§}

[†]*Beijing Engineering Research Centre of Cellulose and Its Derivatives, School of Materials Science and Engineering, Beijing Institute of Technology, 100081, Beijing, P.R. China*

[‡]*Univ. Grenoble Alpes, CNRS, CERMAV, 38000 Grenoble, France*

[¶]*Department of Materials Science, Shanghai University*

[§]*Department of Fiber and Polymer Technology, Wallenberg Wood Science Center, KTH Royal Institute of Technology, Teknikringen 56, 10044 Stockholm, Sweden*

^{||}*Contributed equally to this work*

E-mail: panchen@bit.edu.cn; yoshi@cermav.cnrs.fr; jacke@kth.se

Abstract

The elastic tensors of chitin and chitosan allomorphs were calculated using density functional theory (DFT) with and without dispersion correction, and compared with experimental values. The longitudinal Young's moduli were 114.9 GPa or 126.9 GPa for α -chitin depending on hydrogen bond pattern, 129.0 GPa for β -chitin, and 191.5 GPa for chitosan. Furthermore, the moduli were found to vary between 17.0 to 52.8 GPa in the

1 transverse directions, and between 2.2 to 15.2 GPa in shear. Switching off the dispersion
2 correction lead to a decrease in modulus by up to 63%, depending on the direction. The
3 transverse Young's moduli of α -chitin strongly depended on the hydroxylmethyl group
4 conformation coupled with the dispersion correction, suggesting a synergy between
5 hydrogen bonding and dispersion interactions. The calculated longitudinal Young's
6 moduli were in general higher than experimental values obtained in static conditions
7 and Poisson's ratios were lower than experimental values obtained in static conditions.

8 **Introduction**

9 Chitin is a linear natural polymer consisting of β -1,4 linked N-acetyl-glucosamine, which can
10 be seen as an analogue to cellulose with the N-acetylamino group substituting the hydroxyl
11 group in the C2 position. It is biosynthesized by various living organisms and is found
12 as structural component in, e.g., the exoskeleton of arthropods, and in the cell wall of
13 fungi and yeast.¹ By deacetylation, anhydro-N-acetyl-glucosamine residues can be converted
14 to anhydro-glucosamine and its polymer β -1,4-linked glucosamine, or chitosan. Industrial
15 chitosan is usually a randomly deacetylated product and is not necessarily deacetylated to
16 100%. However, structural studies are usually done on 100% deacetylated samples which is
17 a homopolymer of glycosamine residue.

18 One particular aspect of chitin and chitosan compared to cellulose is their bioresorbability.
19 While cellulose cannot be metabolized by mammalians, including humans, both chitin and
20 chitosan can be degraded inside the mammalian body giving them an important advantage
21 over cellulose for biomedical applications. The intrinsic mechanical properties, e.g. stiffness,
22 are another attractive aspect² of chitin and chitosan, which becomes important in the context
23 of bio-based functional materials.

24 Depending on its biological origin, the chitin polymer chain is usually assembled into
25 either of the two crystalline allomorphs, namely α -chitin³ and β -chitin.⁴ The main difference
26 between them is the chain polarity, which is antiparallel in α -chitin and parallel-up in β -

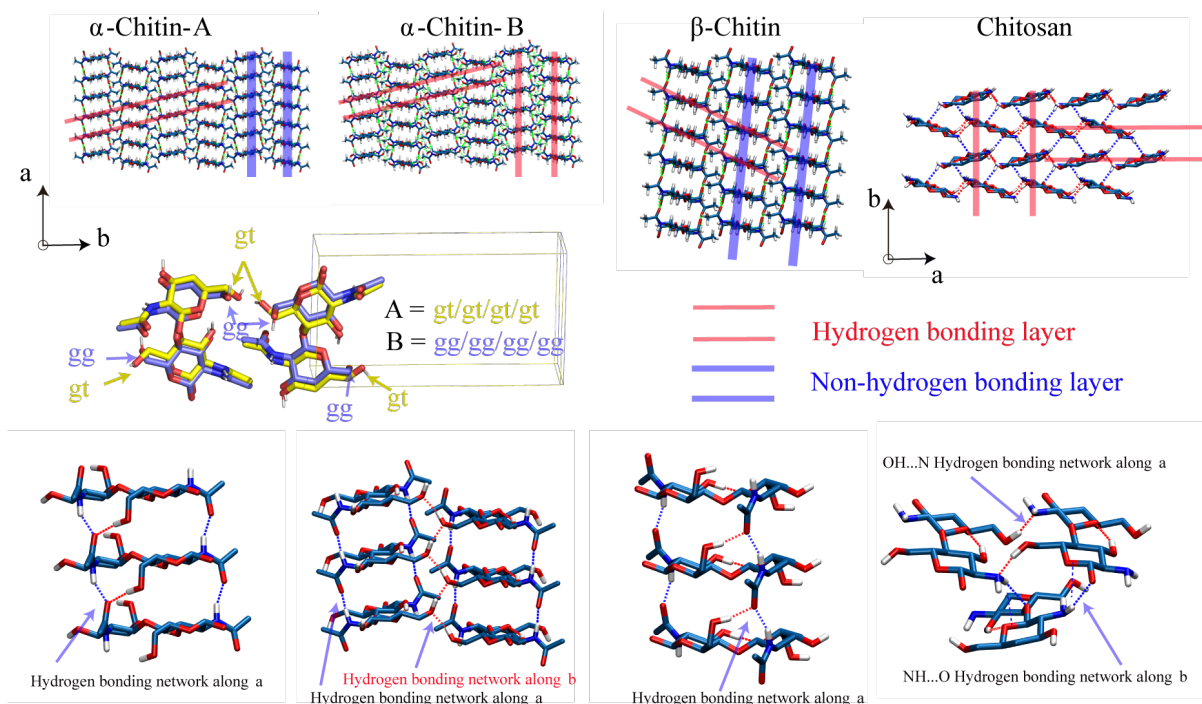


Figure 1: Structural details of α -chitin-A, α -chitin-B, β -chitin, and chitosan. The upper four snapshots present the cross-section morphology. The middle one shows the hydroxymethyl isomerization in α -chitin-A and α -chitin-B. The bottom ones illustrate the HB network.

1 chitin.⁵ In both cases, they form crystalline microfibrils of nanometer-sized lateral dimension,
 2 similar to native cellulose. Fully deacetylated chitosan can be prepared from chitin in solid
 3 state keeping the macroscopic arrangement.⁶ Structural studies are carried out on model
 4 systems of high crystalline form that are thus either fully N-acetylated or fully deacetylated.

5 The longitudinal modulus is of interest since the function of these fibrils primarily is to
 6 sustain tensile loads in structural and functional materials. Furthermore, the longitudinal
 7 modulus is the least difficult one to approach experimentally. There are two reports of
 8 the crystal modulus of α -chitin, one for chitosan and none for the β -chitin. Using X-ray
 9 diffraction, Nishino et al.⁷ reported a longitudinal modulus of 41 and 65 GPa of the crystalline
 10 regions in α -chitin and in chitosan, respectively. They also concluded the modulus of α -chitin
 11 to be constant in the temperature range -190 to 150 °C. Using a similar approach, Ogawa et
 12 al.⁸ reported a slightly higher value of 59.3 ± 11.3 GPa for α -chitin.

13 Transverse mechanical properties and shear modulus are also important as the crystals

1 are subject to complex stress environments, both in their native setting (in the case of
2 chitin) and during processing. In addition to the experimental studies mentioned above, the
3 mechanical properties of chitin have been investigated using atomistic and coarse-grained
4 force-field based molecular dynamics simulation,⁹⁻¹² but determination of the full elastic
5 tensors has not yet been reported.

6 Poisson’s ratio is another interesting parameter to look at, since the measurement is
7 less prone to artifact and uncertain assumptions. Even if stress transfer in the material or
8 accurate measurement of the cross-sectional area is challenging, the Poisson’s ratio does not
9 depend on the absolute value of stress on the sample and can be robust.

10 In our recent study, we analyzed the effect of dispersion interactions on cellulose crys-
11 tals,¹³ by switching the dispersion correction^{14,15} on and off. Here we apply the same ap-
12 proach to chitin and chitosan. For α -chitin the naturally occurring isomerization of the
13 hydroxymethyl group¹⁶ (here denoted α -chitin-A and α -chitin-B, see computational details)
14 further allowed us to analyze the contribution of hydrogen bonds (HBs) on the elastic mod-
15 ulus was quantified.

16 Computational method and experimental section

17 Periodic DFT calculations were performed using the quantum espresso package (version
18 6.6)^{17,18} either with or without applying pairwise DFT-D2 correction.¹⁹ The ElaStic package
19 was used for the estimation of the elastic tensors.^{20,21} Initial crystal coordinates were derived
20 from X-ray and neutron data.^{3,4,6,22} Three crystals, namely, α -chitin, β -chitin, and chitosan,
21 in their anhydrous form, were considered in this work. Due to the hydroxymethyl group
22 induced structural complexity of α -chitin, two different structures of α -chitin taken from the
23 DFT optimization of Deringer et al.¹⁶ were considered, denoted α -chitin-A (*gt* for O6 in four
24 anhydrous N-acetyl-glucosamine residues, shown in Figure 1), and α -chitin-B (*gg* for four
25 O6) respectively. A third one, with mixed *gg* and *gt* for O6, departed from the orthorhombic

1 unit cell during geometry optimization and was thus abandoned. A k-grid of $2 \times 2 \times 2$ was
2 applied to α -chitin-A, α -chitin-B, β -chitin, and chitosan. The kinetic energy cutoff was 160
3 Ry. The convergence threshold of total energy and forces for ionic minimization are $1.0\text{e-}6$
4 Ry and $1.0\text{e-}5$ Ry/bohr, respectively. Periodic calculations were carried out using Quantum
5 Espresso (version 6.6)^{17,18} in combination with ElaStic,^{20,21} a universal tool for calculating
6 elastic constants from first principles. Both α -chitin and chitosan have orthorhombic unit
7 cells,^{3,6} while β -chitin⁴ has a monoclinic one. The elastic tensor was determined using the
8 energy-strain approach. Here, 9 (orthorhombic) or 13 (monoclinic) combinations of strain
9 deformations were applied to deduce the corresponding 9 or 13 tensor elements. For each
10 strain deformation, 11 frames with the strain amplitude varying linearly from -0.01 to 0.01
11 were optimized with fixed unit cell and the energy fitted with a parabolic function. To
12 visualize the feature of calculated elastic tensors, the tensors were further decomposed into 6
13 eigenvalues λ_i and 6 pairs of eigentensors of stress and strain equivalent where $\sigma_i = \lambda_i \epsilon_i$. The
14 stress/strain tensors have 6 independent components and can be visualized by 3D surface
15 contour plots as proposed in PASCAL software.²³ The plots were generated using the online
16 Anisotropic calculator from Zuluaga et al.²⁴ and further processed using the PARAVIEW
17 software.²⁵

18 The experimental Poisson's ratio was obtained from the displacement of the diffraction
19 spots in previous studies of crystal moduli measurements.⁸ The X-ray diffraction strain
20 measurement of β -chitin was carried out by using extracellular crystalline filaments from
21 *Thalassiosira weissflogii* embedded in PVA, following the same protocol and analysis as recent
22 study on cellulose.²⁶ The strain of d-spacings of equatorial spots with respect to the strain
23 meridian spots are also shown in Fig S1 and S2.

Table 1: Elastic tensor elements of chitin and chitosan crystals with or without of dispersion correction. The unit is GPa.

		Stiffness tensor (GPa)											
		C11	C12	C13	C14	C15	C16						
		C12	C22	C23	C24	C25	C26						
		C13	C23	C33	C34	C35	C36						
		C14	C24	C34	C44	C45	C46						
		C15	C25	C35	C45	C55	C56						
		C16	C26	C36	C46	C56	C66						
		Disp correction						No disp correction					
α -chitin-A	27.8	4.5	1.3	0	0	0	21.7	1.2	1.6	0	0	0	
		30.6	6.1	0	0	0		12.6	2.9	0	0	0	
			126.9	0	0	0			110.4	0	0	0	
				10.1	0	0				5.7	0	0	
					3.9	0					3.4	0	
						4.6						3.3	
α -chitin-B	26.4	8.4	2.3	0	0	0	16.4	-1.8	1.1	0	0	0	
		52.8	4.1	0	0	0		26.2	4.6	0	0	0	
			114.9	0	0	0			115.3	0	0	0	
				14.8	0	0				11.3	0	0	
					2.2	0					2.6	0	
					5.3						4.3		
β -chitin	21.9	5.7	5.9	0	0	-1.8	17.8	3.6	4.1	0	0	-1.3	
		17.0	7.6	0	0	4.1		9.9	5.6	0	0	0.7	
			129.0	0	0	3.6			106.4	0	0	0.2	
				15.2	1.2	0				6.9	-0.0	0	
					4.1	0					3.9	0	
					4.0						3.4		
chitosan	24.4	17.1	12.7	0	0	0	18.8	4.3	8.0	0	0	0	
		27.5	8.7	0	0	0		10.1	3.0	0	0	0	
			191.5	0	0	0			142.6	0	0	0	
				3.5	0	0				2.4	0	0	
					10.1	0					7.6	0	
					4.3						3.2		

1 Result and discussion

2 Estimation of stiffness tensor from DFT calculation

3 Table 1 shows calculated elastic tensor elements of the four crystals. The one corresponding
4 to longitudinal deformation C33 was 126.9 and 114.9 GPa for α -chitin in the two different
5 hydroxymethyl group conformations (A and B, respectively). It was 129.0 GPa for β -chitin,
6 and 191.5 GPa for chitosan. The corresponding longitudinal Young’s moduli, calculated
7 as $1/S_{33}$ from the compliance matrix S_{ij} (see Table S1 and S2) were 125.6, 114.4, 122.7,
8 and 184.8 GPa, respectively. Simulated moduli are indeed much higher than experimentally
9 determined values (41 and 59.3 ± 11.3 GPa⁷ and 65 GPa,⁸ using two different X-ray tech-
10 niques). This difference is probably related to the low off-diagonal elements calculated by
11 DFT.²⁶ In reality, when the fibril is stretched in the axial direction, the lateral dimension
12 decreases to keep the volume unchanged, and thus the energy increase is attenuated. This
13 process is probably slow and the molecular deformation to accommodate the available space
14 might be incompatible with strict periodicity in all directions. The experimental estimates
15 for chitin and chitosan by Nishino et al.⁷ look reasonable especially as the f -value, i.e. the
16 modulus multiplied by the chain cross-sectional area, are similar. Also in previous DFT
17 calculations on crystalline cellulose, moduli were high compared to the static deformation
18 experiments,^{26,27} and the simulated Poisson’s ratio was low even in classical MD calcula-
19 tion.²⁸ Thus, there are definitely limitations for both DFT and classical MD approaches.

20 Figure 1 shows the molecular structures of the four crystals. Chain polarity is antiparallel
21 in both α -chitin and chitosan, and parallel-up in β -chitin. Both β -chitin and chitosan have
22 their hydrated crystalline forms, but not α -chitin. The interchain HB network only extended
23 along the a -axis within a single molecular sheet, but not within the sheets parallel to the
24 b -axis, in both α -chitin-A and β -chitin. In both α -chitin-B and chitosan, however, the
25 interchain HB network extended along both the a and b axes simultaneously.

26 Transverse elastic constants varied from 17.0 to 52.8 GPa and the shear moduli were in

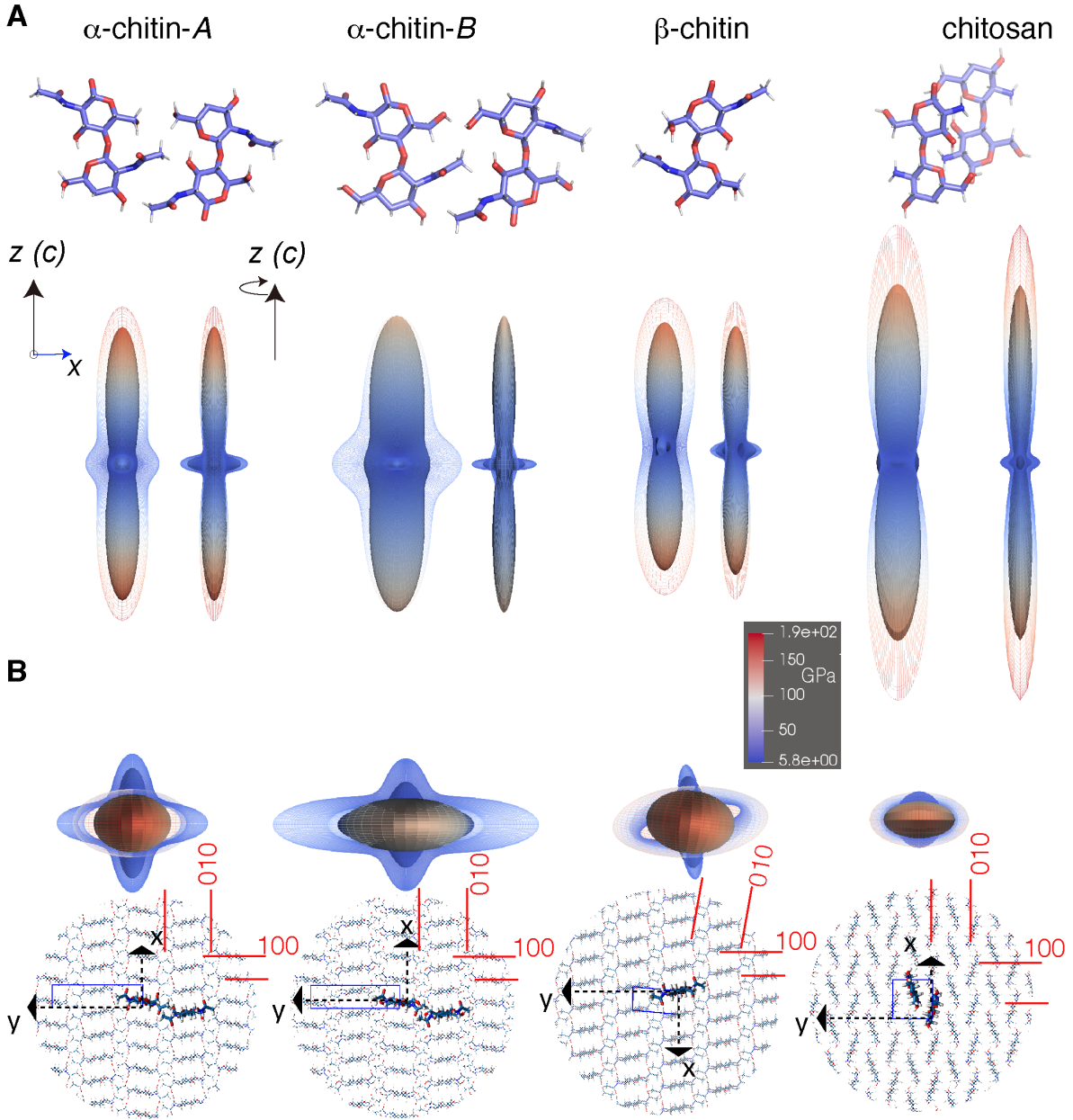


Figure 2: 3D representation of the elastic modulus isosurfaces of crystalline chitin and chitosan with (grid contour) or without dispersion correction (solid contour) from two different perspectives, the isosurfaces in B is enlarged for α -chitin-A, α -chitin-B, β -chitin, chitosan, for better visualization. The views of two crystalline chitin allomorphs and chitosan labeled with unit cell and deformation vectors as well as the corresponding characteristic crystalline planes. The cross-section snapshots of each crystal are shown in the same viewing angle as the corresponding iso-surface in B. The unit cell parameter a is parallel to x , c is parallel to z , and y lies in the ab plane.

1 the range 2.2 GPa to 15.2 GPa (Table 1), both of which are much smaller than that of the
 2 longitudinal ones, indicating strong anisotropy in all crystals.

Table 2: The unit cell parameters of crystalline α -chitin,³ β -chitin,⁴ and chitosan,²² from experiment and DFT calculation.⁶ Lengths in Å, angles in degrees and volumes in Å³. The difference in percentage is calculated through (No disp.-Expt.)/Expt. \times 100%.

		a	b	c	α	β	γ	Volume
α -chitin-A	Expt. ³	4.749	18.890	10.33	90.0	90.0	90.0	926.7
	Disp.	4.587	18.495	10.32	90.0	90.0	90.0	875.5
	No disp.	4.908	19.591	10.43	90.0	90.0	90.0	1002.9
	Rel. incr.	3.3%	3.7%	1.0%				8.2%
α -chitin-B	Expt. ³	4.749	18.890	10.33	90.0	90.0	90.0	926.7
	Disp.	4.656	18.166	10.33	90.0	90.0	90.0	873.7
	No disp.	4.971	18.953	10.47	90.0	90.0	90.0	986.4
	Rel. incr.	4.7%	0.3%	1.4%				6.4%
β -chitin	Expt. ⁴	4.819	9.239	10.38	90.0	90.0	97.2	458.5
	Disp.	4.725	8.952	10.36	90.0	90.0	95.3	436.3
	No disp.	4.969	9.791	10.44	90.0	90.0	98.7	502.1
	Rel. incr.	3.1%	6.0%	0.6%				9.5%
chitosan	Expt. ²²	8.129	8.347	10.31	90.0	90.0	90.0	699.6
	Disp.	7.942	8.173	10.37	90.0	90.0	90.0	673.1
	No disp.	8.217	8.855	10.44	90.0	90.0	90.0	759.6
	Rel. incr.	1.1%	6.1%	1.3%				8.6%

3 Influence of Dispersion Energy

4 With dispersion correction switched off, the estimated volume of the unit cell increased by
 5 5-9%, and most of the unit cell parameters expanded (Table 2), indicating a relative looser
 6 assembly of macromolecular chains than with dispersion correction switched on. At the same
 7 time, estimated elastic constants decreased between -18% to -63% depending on the unit cell
 8 direction (see Figure 1 and Table 1). The largest decrease occurred in the direction of the b -
 9 axis for all crystals (except for α -chitin-B), which is normal to the glucosamine ring plane for
 10 chitosan, but parallel to the acetylated glucosamine ring plane in both α -chitin and β -chitin
 11 (Figure 1). It is interesting to note that the E33 of α -chitin-B is not affected by switching
 12 off dispersion correction. The relative decrease was smaller along the unit cell a -axis due to

1 the resistance from the interchain HB network, which strengthens chain association in that
2 direction, as discussed in detail below.

3 **Contribution from HB**

4 From a structural perspective, both the O6-HO6 group and the nearby N2-H2 group in
5 α -chitin-A orient themselves toward the oxygen in the C=O groups, thus forming a dual
6 HB between the (100) planes and within (010) sheets, while the *gt* conformation of the
7 hydroxymethyl group prohibits HBs between (010) planes. In the other form, α -chitin-B,
8 in which O6 is found in the *gg* conformation, the N2-H2...O=C HBs dominate within the
9 (010) planes, while O6HO6...O6 HBs are present between (010) planes (See Figure 1). Such
10 different OH isomerization leads to different density of interchain HBs between adjacent
11 (010) planes in A and B: one per anhydrous glucosamine residue in type B and zero in type
12 A respectively (see Table 3 and Figure 3). The HB density between (100) planes within
13 the same (010) sheet is also different between the A and B. It is two per residue in the A
14 form and one per residue in B. These differences in HB pattern originating from different
15 conformations lead to significant differences for the elastic tensor in the transverse direction.
16 As shown in Figure 1, and in both Table 1 and Table 3, the effects from HBs and dispersion
17 energy on the transverse modulus are coupled. A nearly two-fold difference in E22 (30.6
18 versus 52.8 GPa) is observed between α -chitin-A and α -chitin-B. By switching off dispersion
19 correction while retaining the HO6...O6 interchain HBs, these two values reduce to 12.6 and
20 26.2 GPa, respectively. On the other hand, E11 is 27.8 and 26.4 for A and B, respectively,
21 and decreases to 21.7 and 16.4 as the dispersion correction is cancelled, thus showing much
22 smaller reduction. Therefore, in the direction with more HBs, cancellation of dispersion leads
23 to larger reduction of the modulus. This is because the HBs lead to tighter chain assembly
24 and hence larger dispersion interaction.

25 The effect of HBs on the moduli can be further estimated by comparison between cellulose
26 I β and α -chitin. The number of HBs between two chains within the (200) plane of cellulose

Table 3: Effect of HB density (number of HBs per anhydrous glucan residue) and dispersion correction on transverse elastic modulus E (GPa).

	E22			E11		
	α -chitin-A	α -chitin-B	B-A	α -chitin-A	α -chitin-B	B-A
HB density	0	0.5	0.5	2	1	-1
E (Disp)	30.6	52.8	22.2	27.8	26.4	-1.4
E (No disp)	12.6	26.2	13.6	21.7	16.4	-5.3
ΔE	+18.0	+26.6	+8.6	+6.1	+10.0	+3.9

1 $I\beta$ is one per glucose residue. For α -chitin-A and B within the (110) and (1-10) planes, this
2 number is zero and one respectively. Although the HB density is the same between cellulose
3 $I\beta$ and α -chitin-B. The HB directions in $I\beta$ is perfectly parallel to the (200) plane whereas
4 the (110) and (1-10) planes in α -chitin-B both showed a tilt angle of 15° with respect to
5 the (100) plane. Therefore the “effective” HB density that contributes to C22 is less than
6 one per residue. The Young’s modulus decreased monotonously as the density of interchain
7 HBs decreased (Figure 3), and was calculated to 99.2, 52.8, and 30.6 GPa, respectively.¹³
8 With dispersion switched off, these values decreased to 68.2, 26.2, and 12.6 GPa, thus being
9 reduced by 31.0, 26.6, and 18.0 GPa, respectively. Along the chain staggering direction (010
10 plane), the HB density is 0, 1, and 2 for $I\beta$, α -chitin-B, and α -chitin-A. Here, C11 increased
11 monotonously as 17.6, 26.4, and 27.8 GPa with dispersion on, and 5.3, 16.4, 21.7 GPa with
12 dispersion off.

Table 4: The elastic tensile and shear modulus of chitin and chitosan (GPa).

	Disp correction				No disp correction			
	α -chitin-A	α -chitin-B	β -chitin	chitosan	α -chitin-A	α -chitin-B	β -chitin	chitosan
E11	27.8	26.4	21.9	24.4	21.7	16.4	17.8	18.8
E22	30.6	52.8	17.0	27.5	12.6	26.2	9.9	10.1
E33	126.9	114.9	129.0	191.5	110.4	115.3	106.4	142.6
G23	10.1	14.8	15.2	3.5	5.7	11.3	6.9	2.4
G13	3.9	2.2	4.1	10.1	3.4	2.6	3.9	7.6
G12	4.6	5.3	4.0	4.3	3.3	4.3	3.4	3.2

13 Besides the non-covalent interactions, the modulus along one specific transverse direction
14 is also partially governed by the covalent bonds. With dispersion correction applied, the es-

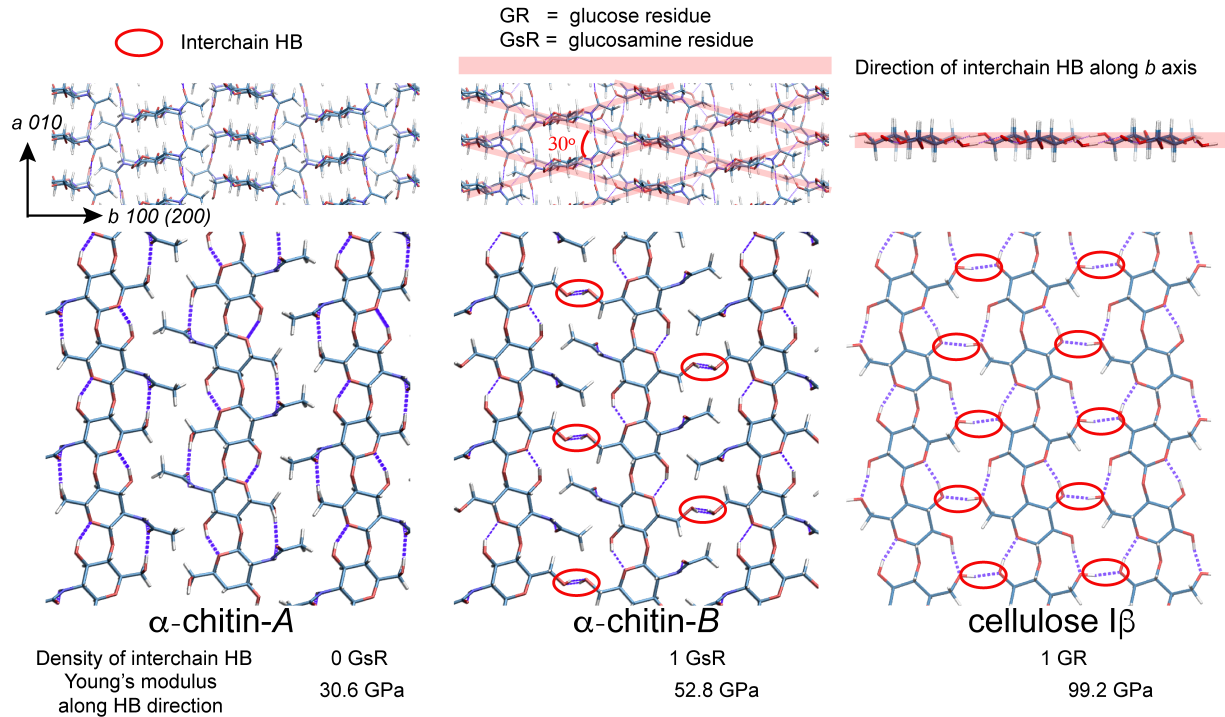


Figure 3: Illustration of interchain HB patterns and numbers in α -chitin-A, α -chitin-B, and cellulose I β .

1 timated transverse modulus is larger in the direction of high covalent bond density, as can be
 2 seen by comparing E_{11} and E_{22} in Table 4. However, the contribution of HBs and dispersion
 3 energy as well as the covalent bonds to elastic modulus is strongly correlated and cannot
 4 be decomposed in a simple way. For instance, one cannot conclude that HBs contribute a
 5 certain percentage to the stiffness by (artificially) removing the HBs and calculate the mod-
 6 ulus. This is because of (1) removing HBs also alters other parameters simultaneously (chain
 7 packing etc.) that affects the stiffness too, and (2) separate contributions to the stiffness are
 8 not necessarily additive. However, if one scales the absolute difference in modulus by the
 9 number of HBs in that direction, one finds that the contribution from dispersion interaction
 10 to the elastic mechanical properties is comparable to that from HBs, both along the b and a
 11 axis of α -chitin.

12 The HB pattern in β -chitin is similar to that in α -chitin-A. The difference between the
 13 two allomorphs is (1): the adjacent molecular chains, which are anti-parallel in the α , but

1 parallel in β , and (2): the chain packing, which gives a zig-zag patterned cross-section in α ,
2 and a more planar arrangement in β . The longitudinal modulus of the two forms are almost
3 the same (126.9 GPa versus 114.9 GPa) due to the same β -1,4-glycosidic linkages, the same
4 intrachain HO3...O5 HBs along the chain direction, as well as similar density. However, the
5 transverse modulus is slightly smaller for the β form. In the elastic tensor surface in Figure
6 2B, one recognizes that the maximum elastic constant around x and y axis (Figure 1) in the
7 cross-section is similar for α -chitin-A and β -chitin.

8 The higher longitudinal modulus E33 of chitosan compared to the other crystals (Table
9 4) is partly due to more efficient chain packing leading to higher number of chains per unit
10 area, but after normalization by volume it is still about 17% higher than the stiffest chitin
11 allomorph.

12 **Energy decomposition**

13 Several numerical methods have been developed specifically for decomposing non-covalent
14 interactions in DFT calculations, such as reduced density gradient²⁹ and independent gra-
15 dient method.³⁰ In the present work, decomposition was achieved using a simpler approach
16 where dispersion and electrostatic energy components were estimated by systematic unit cell
17 enlargement while simultaneously switching the dispersion correction on and off during DFT
18 geometry optimization. As shown in Figure 4, the original unit cell of β -chitin was enlarged
19 by a factor of two in either the a or b direction, or both. With periodic boundary condition
20 applied, this results in four different structures that represent the condensed phase, two dif-
21 ferent cases of separated sheets, and the isolated chains, respectively. These are referred to
22 as 1x1, 2x1, 1x2, and 2x2, respectively (Figure 4). For α -chitin and chitosan, whose unit
23 cells contains two chains, a fifth structure was created by deleting one of the chains in the
24 fully separated case. This structure is here denoted 2x2* (Figure S3 & S4 & S5). The energy
25 difference between these structures is the intermolecular energy needed for the separation of
26 molecular sheets or chains.

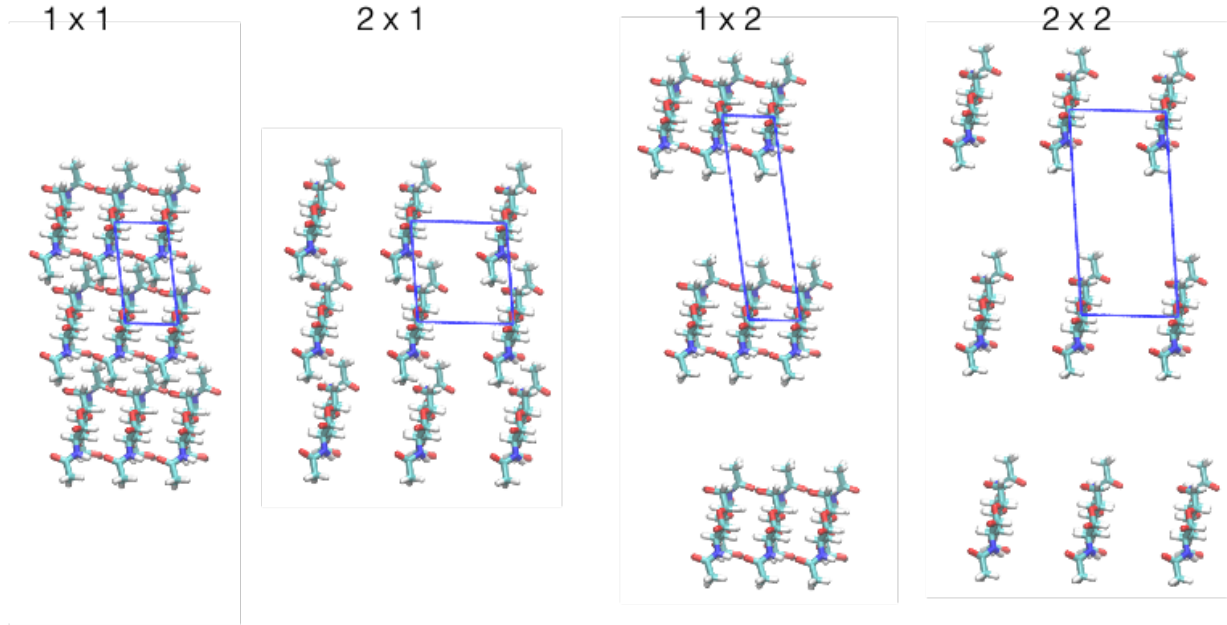


Figure 4: Graphical representation of the four enlarged cells of β -chitin for DFT energy optimization.

1 By switching off and on dispersion correction, eight (or ten) terms of total DFT energies
 2 and four (or five) terms of dispersion correction energies were obtained after energy mini-
 3 mization. These are shown in Table 5. The total energy is split into intra- and inter-chains
 4 energies and further into their respective electrostatic and dispersion contributions. The
 5 total non-covalent interaction is the sum of four components: the inter-chain electrostatic
 6 energy (E_{interE}), the intra-chain electrostatic energy (E_{intraE}), the inter-chain dispersion en-
 7 ergy (E_{interD}), and the intra-chain dispersion energy (E_{intraD}). Since the morphology and
 8 the geometry of the individual polymer chains did not vary significantly, we assume both
 9 E_{intraE} and E_{intraD} to be constant. The E_{intraD} (per unit cell) is -141.87 kJ/mol, calculated
 10 from the 2x2 structure. Since the total dispersion energy, $E_{disp.corr.} = E_{intraD} + E_{interD}$, both
 11 E_{interE} and E_{interD} can be obtained and are presented in Table 5. The results show that
 12 E_{interD} is comparable to E_{interE} . The HB energy can be considered as one part of E_{interE} ,
 13 thus necessarily smaller than the total value. Therefore, we conclude that the intermolecular
 14 dispersion energy is larger than the HB energy in β -chitin. Thus, the dispersion influences

1 the elastic muduli more than HB does. α -chitin and chitosan also follows this pattern as
 2 shown in Table 5.

Table 5: The energy decomposition of chitin and chitosan. * stands for one chain in the unit cell.

Unit cell		Energy (kJ/mol per unit cell)						
		$E_{vdwcorr.}$	$E_{novdwcrr.}$	$E_{disp.corr.}$	E_{InterE}	E_{IntraD}	E_{InterD}	E_{IntraE}
β -chitin	1x1	-370.93	-125.47	-260.77	-110.16	-141.87	-118.90	
	2x1	-313.45	-109.74	-210.77	-103.28	-141.87	-68.30	
	1x2	-180.83	-10.24	-176.81	-4.01	-141.87	-34.94	Very large
	2x2	-146.96	0	-141.87	-5.09	-141.87	0	
α -chitin-A	1x1	-364.82	-118.81	-260.97	-103.84	-140.88	-120.09	
	2x1	-335.89	-111.88	-234.56	-101.34	-140.88	-93.68	
	1x2	-176.28	-7.56	-170.28	-5.99	-140.88	-29.40	Very large
	2x2	-158.47	-3.02	-154.58	-3.88	-140.88	-13.70	
	2x2*	-142.70	0.00	-140.88	-1.82	-140.88	0.00	
α -chitin-B	1x2	-347.00	-96.45	-263.12	-83.88	-136.18	-126.93	
	2x1	-303.09	-82.54	-231.55	-71.54	-136.18	-95.37	
	1x2	-176.83	-20.45	-168.66	-8.17	-136.18	-32.47	Very large
	2x2	-16.133	-6.37	-152.48	-8.85	-136.18	-16.30	
	2x2*	-135.99	0	-136.18	0.19	-136.18	0.00	
Chitosan	1x1	-296.24	-88.26	-224.20	-72.04	-105.26	-118.94	
	2x1	-240.69	-73.53	-172.93	-67.76	-105.26	-67.66	
	1x2	-170.32	-19.60	-156.41	-13.91	-105.26	-51.15	Very large
	2x2	-116.57	-10.45	-128.41	11.85	-105.26	-23.15	
	2x2*	-104.89	0.00	-105.26	0.37	-105.26	0.00	

3 Eigentensor analysis

4 To facilitate the interpretation of the elastic tensor it was decomposed into six independent
 5 second-order stress and strain eigentensors that fulfill the relation $\sigma = \lambda\epsilon$, where λ is a scalar.
 6 If there are no off-diagonal elements in the elastic tensor, the material only responds to the
 7 direction of deformation, and each eigentensor has only one non-zero element. However, the
 8 presence of off-diagonal elements leads to coupling between different modes. The eigentensors
 9 can be graphically represented by surfaces representing the axial stress/strain component in
 10 the corresponding direction.

1 The eigentensors are shown in Figure 5 in the order of the magnitude of the correspond-
2 ing eigenvalues. Simple normal stress/strain gives a single dumbbell shape and pure shear
3 results in two crossed dumbbells of different colors. α -chitin has relatively simple anisotropy
4 with eigenvalues highest for axial deformation along the chain axis followed by b -axis direc-
5 tion which is roughly parallel to the pyranose plane and a -axis. The shear directions are ac ,
6 ab , bc in the descending order of eigenvalues. Strong coupling between two normal directions
7 leads to one doughnut shape and one shear-like component, exemplified by, e.g., the second
8 and third eigenvalues in α -chitin-A with dispersion correction (top row) which correspond to
9 the a and b directions, respectively. Relatively strong coupling in the two directions perpen-
10 dicular to the chain axis can also be seen for the B type without dispersion correction (3rd
11 eigentensor). Also β -chitin and chitosan exhibit strong coupling in the direction perpendic-
12 ular to the chain direction especially with dispersion correction (2nd and 3rd eigentensor for
13 β -chitin and 2nd and 4th eigentensor for chitosan).

14 **Poisson's ratio**

15 The Poisson's ratios for orthorhombic unit cell when stretched along the fiber direction, can
16 be simply defined along the two orthogonal crystallographic axes. They are summarized in
17 table S3. For α -chitin, the experimental value was 0.46 along the b -direction (ν_{32}) whereas
18 the DFT gave 0.06-0.2 depending on the hydrogen bonding pattern, but significantly lower
19 than experimental value in any case. The experimental Poisson's ratio perpendicular to the
20 pyranose plane was 0.045, comparable to DFT values of 0.01-0.08 depending on the hydrogen
21 bond pattern, but small in any case.

22 For monoclinic system, the eigenvectors of deformation orthogonal to fiber direction also
23 have to be determined. For β -chitin, the major axis of Poisson's ratio makes about 70° to the
24 a -axis and 27° to the b -axis, which is almost parallel to the pyranose plane. The corresponding
25 Eigenvalue was 0.5. The minor axis orthogonal to this direction has an Eigenvalue of 0.16.
26 On the other hand, the large absolute value of s_{36} of DFT with dispersion correction indicates

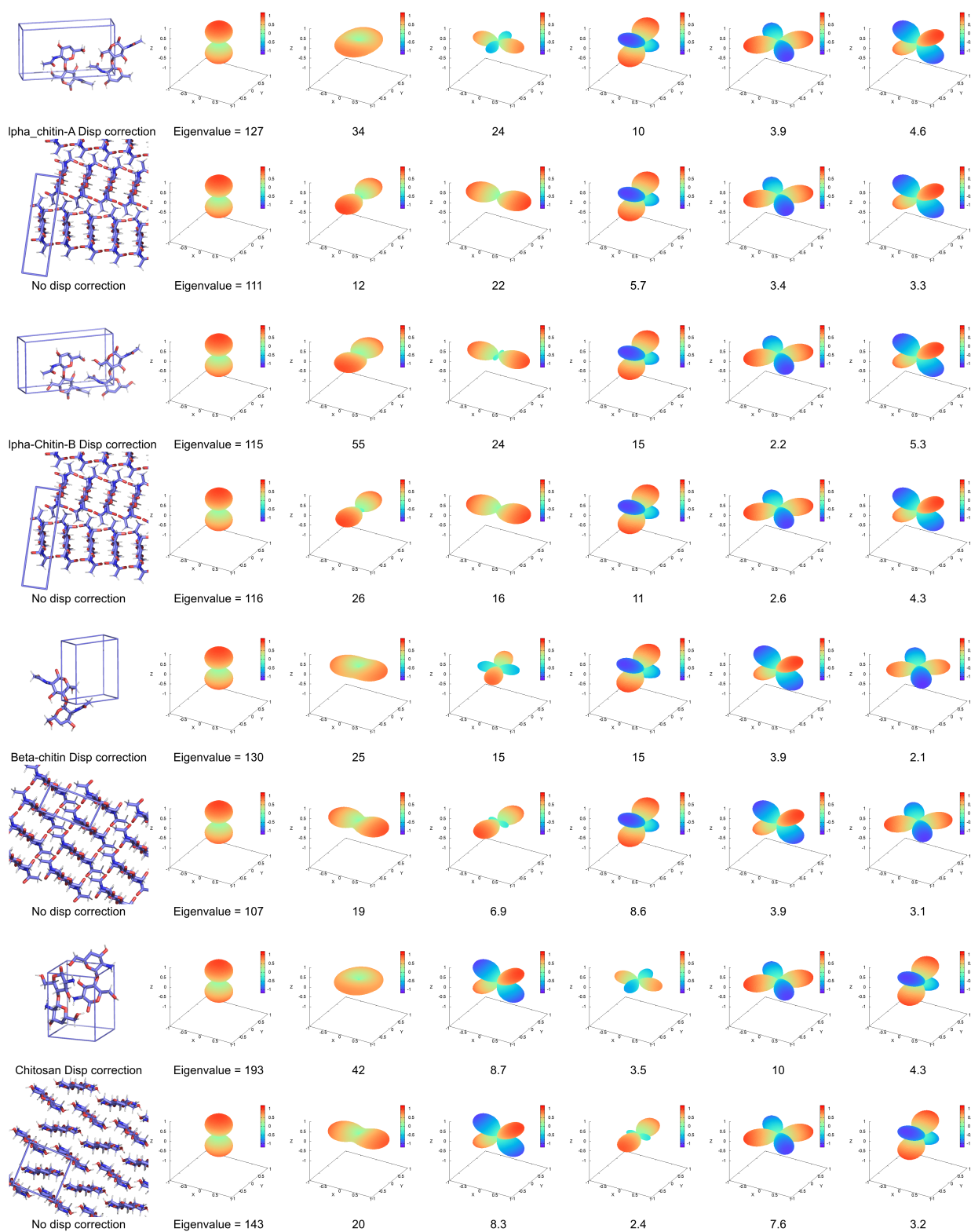


Figure 5: Graphical representation of the unit cells and eigenvalue tensors of α -chitin-A, α -chitin-B, β -chitin, and chitosan with and without dispersion correction.

1 that the axial stress is accompanied by large shear in the ab plane. From another point of
2 view, the Eigenvectors are close to 45° with respect to our reference frame, with Eigenvalues
3 of 0.8 and -0.4. When the dispersion is switched off, s_{36} is close to zero, and the calculated
4 Poisson's ratios are much closer to the experimental value (Table S3).

5 **Conclusion**

6 Using DFT calculations the elastic tensors of α -chitin, β -chitin, and chitosan in their anhy-
7 drous forms were studied. The longitudinal, transverse and shear moduli successively differ
8 by one order of magnitude, with longitudinal modulus $>$ transverse modulus $>$ shear modu-
9 lus. For α -chitin-B, α -chitin-A, β -chitin, and chitosan, the outstanding longitudinal moduli
10 are estimated to be 114.9, 126.9, 129.0, and 191.5 GPa, respectively, indicating their intrinsic
11 potential as structural materials. The transverse moduli (C11 and C22, unit in GPa) are
12 estimated as 52.8 and 27.8, 30.6 and 27.8, 17.0 and 21.9, as well as 27.5 and 24.4 GPa, re-
13 spectively. The shear moduli (C44, C55, C66, unit in GPa) are calculated as (10.1, 3.9, 4.6),
14 (14.8, 2.2, 5.3), (15.2, 4.1, 4.0), and (3.5, 10.1, 4.3), respectively. Switching off the dispersion
15 energy correction reveals a significant contribution from dispersion interaction to mechanical
16 performance, which has often been ignored. The hydroxymethyl group isomerization allows
17 quantification of the contribution of HBs to mechanical properties, which is found to be as
18 important as the contribution from dispersion energy. These findings contribute towards our
19 fundamental understanding of the mechanical properties of crystalline polysaccharides, and
20 are important for explaining structure-property relationships of chitin- and chitosan-based
21 functional materials.

22 **Acknowledgement**

23 P.C. thanks the Beijing Natural Science Foundation (2204096) and Beijing Institute of Tech-
24 nology Research Fund for Young Scholars and BIT-Belarus joint grants. The experiment on

1 β chitin was made possible by the DESY beamtime allocation at Hasylab A2 and Professor
2 Matrin Müller and Dr. Sergio Funari for their help at the beamline. Financial support
3 also came from French National Research Agency (ANR-07-JCJC-0021). We thank Dr. Yu
4 Ogawa from CERMAV for providing the Poisson's ratios measurement of α -chitin.

5 Supporting Information Available

6 Tables of compliance matrices (Table S1 & S2); Poisson's ratios (Table S3); Experimental
7 lattice strain ratio of α -chitin (Figure S1) and β -chitin (Figure S2); Crystal structures in PDB
8 format for α -chitin-A, α -chitin-B, β -chitin, and chitosan.

9 References

- 10 (1) Rinaudo, M. Chitin and Chitosan: Properties and Applications. *Prog. Polym. Sci.*
11 **2006**, *31*, 603–632.
- 12 (2) Duan, B.; Huang, Y.; Lu, A.; Zhang, L. Recent Advances in Chitin Based Materials
13 Constructed via Physical Methods. *Prog. Polym. Sci.* **2018**, *82*, 1–33.
- 14 (3) Sikorski, P.; Hori, R.; Wada, M. Revisit of α -chitin Crystal Structure using High Res-
15 olution X-ray Diffraction Data. *Biomacromolecules* **2009**, *10*, 1100–1105.
- 16 (4) Nishiyama, Y.; Noishiki, Y.; Wada, M. X-ray Structure of Anhydrous β -Chitin at 1 Å
17 Resolution. *Macromolecules* **2011**, *44*, 950–957.
- 18 (5) Ogawa, Y.; Lee, C. M.; Nishiyama, Y.; Kim, S. H. Absence of Sum Frequency Gener-
19 ation in Support of Orthorhombic Symmetry of α -Chitin. *Macromolecules* **2016**, *49*,
20 7025–7031.
- 21 (6) Naito, P. K.; Ogawa, Y.; Sawada, D.; Nishiyama, Y.; Iwata, T.; Wada, M. X-ray Crystal
22 Structure of Anhydrous Chitosan at Atomic Resolution. *Biopolymers* **2016**, *105*, 361–8.

- 1 (7) Nishino, T.; Matsui, R.; Nakamae, K. Elastic Modulus of the Crystalline Regions of
2 Chitin and Chitosan. *J Polym. Sci. B Polym. Phys.* **1999**, *37*, 1191–1196.
- 3 (8) Ogawa, Y.; Hori, R.; Kim, U.-J.; Wada, M. Elastic Modulus in the Crystalline Region
4 and the Thermal Expansion Coefficients of α -chitin Determined using Synchrotron
5 Radiated X-ray Diffraction. *Carbohydr. Polym.* **2011**, *83*, 1213–1217.
- 6 (9) Yu, Z.; Lau, D. Development of a Coarse-grained α -chitin Model on the Basis of MAR-
7 TINI Forcefield. *J Mol. Model.* **2015**, *21*, 128.
- 8 (10) Yu, Z.; Lau, D. Molecular Dynamics Study on Stiffness and Ductility in Chitin–protein
9 Composite. *J Mater. Sci.* **2015**, *50*, 7149–7157.
- 10 (11) Cui, J.; Yu, Z.; Lau, D. Effect of Acetyl Group on Mechanical Properties of
11 Chitin/Chitosan Nanocrystal: A Molecular Dynamics Study. *Int. J Mol. Sci.* **2016**,
12 *17*, 61.
- 13 (12) Wei, A.; Fu, J.; Guo, F. Mechanical Properties of Chitin Polymorphs: A Computational
14 Study. *J Mater. Sci.* **2021**, *56*, 12048–12058.
- 15 (13) Chen, P.; Nishiyama, Y.; Wohlert, J. Quantifying the Influence of Dispersion Inter-
16 actions on the Elastic Properties of Crystalline Cellulose. *Cellulose* **2021**, *28*, 10777–
17 10786.
- 18 (14) Bučko, T.; Hafner, J.; Lebègue, S.; Ángyán, J. G. Improved Description of the Structure
19 of Molecular and Layered Crystals: Ab Initio DFT Calculations with Van Der Waals
20 Corrections. *J Phys. Chem. A* **2010**, *114*, 11814–11824.
- 21 (15) Bučko, T.; Tunega, D.; Ángyán, J. G.; Hafner, J. Ab Initio Study of Structure and
22 Interconversion of Native Cellulose Phases. *J Phys. Chem. A* **2011**, *115*, 10097–10105.
- 23 (16) Deringer, V. L.; Englert, U.; Dronskowski, R. Nature, Strength, and Cooperativity of
24 the Hydrogen-Bonding Network in α -Chitin. *Biomacromolecules* **2016**, *17*, 996–1003.

- 1 (17) Giannozzi, P.; Baroni, S.; Bonini, N.; Calandra, M.; Car, R.; Cavazzoni, C.; Ceresoli, D.;
2 Chiarotti, G. L.; Cococcioni, M.; Dabo, I. *et al.*. QUANTUM ESPRESSO: A Modu-
3 lar and Open-source Software Project for Quantum Simulations of Materials. *J Phys.*
4 *Condens. Matter.* **2009**, *21*, 395502.
- 5 (18) Giannozzi, P.; Andreussi, O.; Brumme, T.; Bunau, O.; Buongiorno Nardelli, M.; Ca-
6 landra, M.; Car, R.; Cavazzoni, C.; Ceresoli, D.; Cococcioni, M. *et al.*. Advanced Capa-
7 bilities for Materials Modelling with Quantum ESPRESSO. *J Phys. Condens. Matter.*
8 **2017**, *29*, 465901.
- 9 (19) Grimme, S.; Antony, J.; Ehrlich, S.; Krieg, H. A Consistent and Accurate Ab Ini-
10 tio Parametrization of Density Functional Dispersion Correction (DFT-D) for the 94
11 Elements H-Pu. *J Chem. Phys.* **2010**, *132*, 154104.
- 12 (20) Yanchitsky, B. Z.; Timoshevskii, A. N. Determination of the Space Group and Unit
13 Cell for a Periodic Solid. *Comput. Phys. Comm.* **2001**, *139*, 235–242.
- 14 (21) Golesorkhtabar, R.; Pavone, P.; Spitaler, J.; Puschnig, P.; Draxl, C. ElaStic: A Tool
15 for Calculating Second-order Elastic Constants from First Principles. *Comput. Phys.*
16 *Comm.* **2013**, *184*, 1861–1873.
- 17 (22) Ogawa, Y.; Naito, P. K.; Nishiyama, Y. Hydrogen-bonding Network in Anhydrous
18 Chitosan from Neutron Crystallography and Periodic Density Functional Theory Cal-
19 culations. *Carbohydr. Polym.* **2019**, *207*, 211–217.
- 20 (23) Cliffe, M. J.; Goodwin, A. L. PASCAL: A Principal Axis Strain Calculator for Thermal
21 Expansion and Compressibility Determination. *J. Appl. Crystallogr.* **2012**, *45*, 1321–1329.
- 22 (24) Zuluaga, M.; Dri, F.; Zavattieri, P.; Moon, R. Anisotropy Calculator - 3D Visualization
23 Toolkit. **2014**,

- 1 (25) Ahrens, J.; Geveci, B.; Law, C. ParaView: An End-User Tool for Large Data Visual-
2 ization. *Visualization Handbook* **2005**, 717–731.
- 3 (26) Song, G.; Lancelon-Pin, C.; Chen, P.; Yu, J.; Zhang, J.; Su, L.; Wada, M.; Kimura, T.;
4 Nishiyama, Y. Time-Dependent Elastic Tensor of Cellulose Nanocrystal Probed by
5 Hydrostatic Pressure and Uniaxial Stretching. *J Phys. Chem. Lett.* **2021**, *12*, 3779–
6 3785.
- 7 (27) Dri, F. L.; Hector, L. G.; Moon, R. J.; Zavattieri, P. D. Anisotropy of the Elastic Prop-
8 erties of Crystalline Cellulose *I_{beta}* from First Principles Density Functional Theory
9 with Van Der Waals Interactions. *Cellulose* **2013**, *20*, 2703–2718.
- 10 (28) Wohlerlert, J.; Bergensträhle-Wohlerlert, M.; Berglund, L. A. Deformation of Cellulose
11 Nanocrystals: Entropy, Internal Energy and Temperature Dependence. *Cellulose* **2012**,
12 *19*, 1821–1836.
- 13 (29) Johnson, E. R.; Keinan, S.; Mori-Sánchez, P.; Contreras-García, J.; Cohen, A. J.;
14 Yang, W. Revealing Noncovalent Interactions. *J Am. Chem. Soc.* **2010**, *132*, 6498–
15 6506.
- 16 (30) Lefebvre, C.; Rubez, G.; Khartabil, H.; Boisson, J.-C.; Contreras-García, J.; Hénon, E.
17 Accurately extracting the signature of intermolecular interactions present in the NCI
18 plot of the reduced density gradient versus electron density. *Phys. Chem. Chem. Phys.*
19 **2017**, *19*, 17928–17936.

1 TOC Graphic

2

